sustainability

MDPI

Article

Seismic Performance of a Sliding Isolation Bridge System with a New Spring Re-Centering Device

Pengcheng Yin [1], Jianguo Wang [2,*] and Yutao Pang [3]

[1] China Railway Siyuan Survey and Design Group Co., Ltd., Heping Avenue 745, Wuhan 430074, China
[2] Department of Civil, Geological and Mining Engineering, Polytechnique Montréal, Montréal, QC H3C 3A7, Canada
[3] Faculty of Engineering, China University of Geosciences, Lumo Road 388, Wuhan 430074, China
* Correspondence: jianguo.wang@polymtl.ca

Abstract: Residual displacements between the girder and piers were observed in previous strong earthquakes. These are caused by the limited re-centering capacity of sliding isolation bearings. With this concern, a spring re-centering device is proposed to improve the re-centering capacity of sliding isolation systems. The working mechanism is illustrated, and the force–deformation relationship of this device was investigated in theoretical, experimental, and finite element methods. An extra-dosed multi-pylon cable-stayed bridge was introduced to demonstrate the re-centering effect. The results show that this spring re-centering device could slightly mitigate the seismic forces and significantly mitigate the residual displacement between the girder and piers. After that, the parametric analysis was conducted to investigate the effect of critical parameters of re-centering bearings on seismic performances.

Keywords: spring re-centering device; lateral stiffness of spring; sliding isolation system; relative and residual displacements; optimal design

Citation: Yin, P.; Wang, J.; Pang, Y. Seismic Performance of a Sliding Isolation Bridge System with a New Spring Re-Centering Device. *Sustainability* **2022**, *14*, 10720. https://doi.org/10.3390/su141710720

Academic Editors: Ning Zhang, Shuai Li, Denghui Dai and Xin Chen

Received: 3 August 2022
Accepted: 22 August 2022
Published: 29 August 2022

1. Introduction

The isolation design method is regarded as one of the best choices during modern bridge seismic design [1–5]. As a result, seismic isolation bearings have been broadly used in practical engineering [6–10]. The isolation systems can be classified into three categories: (a) spring like isolation bearings, i.e., laminated and leader rubber bearings; (b) sliding isolation bearings, such as pendulum and pot isolation bearings; and (c) a combination of the previous two bearing types [1]. They could limit the inertia force transferring to the structure, and dissipate seismic energy due to their specific energy dissipation mechanism. Among these isolation systems, sliding isolation bearings are widely used because of financial and construction concerns [11–13]. However, sliding isolation has low re-centering capability, which then leads to excessive relative and residual displacements after strong earthquakes [14–16]. The large displacement will affect the functionality and resilience of the bridges [17] and cause a high probability of severe pounding damage and unseating failure when the clearance and supporting width are not enough.

Due to this shortcoming, previous studies have proposed many methods to improve the re-centering capacity of a sliding system. Some researchers [18–20] have introduced variable frequency pendulum isolators associated with variable curvatures (SIVC), friction coefficients, and sliding surfaces. Other researchers proposed embodying additional re-centering elements [21–25] to improve the re-centering capacity. For example, Mostaghel and Khodaverdian [21] and Zayas et al. [22] combined the sliding isolation bearing with a friction-based restoring pendulum system. Haque et al. [23] and Cao et al. [24,25] applied super-elastic memory alloys to improve systematic re-centering capacity. Ozbulut [26] combined re-centering SMA with a variable friction damper to mitigate the residual story drift. Generally, these methods can improve the re-centering capacity to some extent, but

they usually bring financial or technical challenges. With this concern, a re-centering device that is simple to construct and economically friendly will be more broadly welcomed.

Theoretically, the re-centering is realized by a restoring force when the relative displacement between adjacent components deviates from its original equilibrium position. This will be improved if the restoring force proportionally relates to the relative deviating. In this regard, springs with very elastic properties can be used as typical materials to improve the re-centering capacity. Due to this reason, some researchers have recently introduced springs to improve re-centering capacities. Kitayama and Constantinu [27,28] and Constantinou et al. [29,30] proposed a sliding isolation system consisting of Teflon disc bearings and helical steel springs to improve re-centering capacity; Chakraborty [1] combined conical springs with flat sliding bearings to limit the peak and residual displacements; Xu et al. [31] introduced pre-pressed disc springs to the system of friction energy dissipation devices. Khoo et al. [32] developed a self-centering device generated by combining ring springs and asymmetrical friction connections. These springs provide re-centering force by compression and tension deformation in their axial direction. Unfortunately, the space at top of the pier is usually limited and it is hard to get an ideal resistant stiffness for an effective re-centering capacity [33–35]. Additionally, since these springs are directly connected to superstructures and substructures, these springs will deform with the varying of temperature. Such deformation not only introduces fatigue damage to the spring but also causes additional force to the bridge pier. However, it has been found that the spring can also provide restoring stiffness in the lateral direction and such stiffness could also be used to improve the re-centering capacity.

The current study aims to propose a new spring re-centering device that employs the lateral stiffness of springs and effectively restrains the relative and residual displacement between the girder and piers. The components and working mechanism of this device are carefully illustrated and the force-displacement relationship for numerical analysis is derived. Then, time-history analyses are conducted to evaluate their effect on seismic responses based on an extra-dosed cable-stayed bridge. Finally, an optimal analysis is conducted to investigate the influence of these re-centering device parameters on seismic responses.

2. Re-Centering Spring Device

2.1. Working Mechanism

As shown in Figure 1, the spring re-centering device is composed of three parts: spring, rubber, and the base system. In this re-centering device, the spring has a rectangular cross-section. The re-centering stiffness is changed by composing multilevel springs with different nominal diameters, which are nested on a flange with several layers. All of these springs are considered to be reliably connected to the base system (the upper and bottom plates), i.e., welded to the flange. Then, the spring system is covered by rubber which protects the spring system from erosion and ensures the spring's stability. Additionally, the reinforced rubber also provides resisting stiffness when the spring re-centering device deforms laterally.

The spring re-centering device is designed to mitigate the residual displacement between the girder and piers during excessive earthquake excitations. To decrease the influence on the bridge's daily working state, the new spring re-centering device was constructed with a free distance, which is used to adjust general temperature deformations. This free distance was realized by setting an elliptical anchorage hole on the upper plate, which was determined by the bridge's creep effect and the acceptable relative displacement between the girder and piers. Thus, the bolt which is fixed to the deck could move in the hole, but will be restrained from excessive relative displacement.

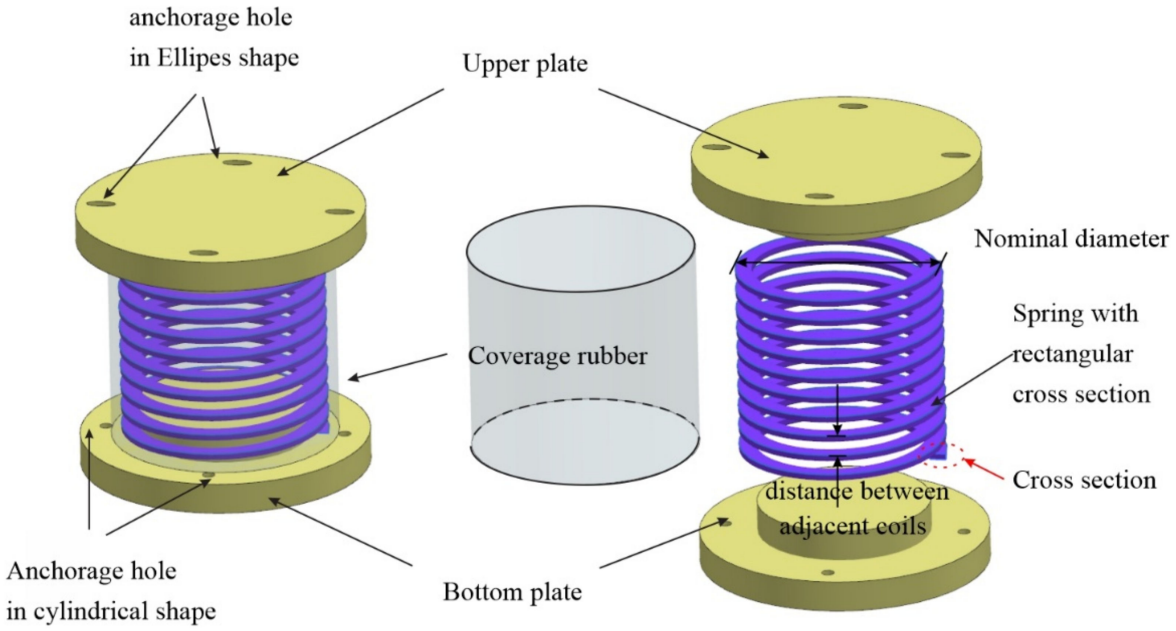

Figure 1. The sketch of proposed spring re-centering device.

2.2. Force–Displacement Relationship

The force–displacement relationship of the new spring re-centering device can be divided into multiple stages. For example, when the relative displacement is small, the spring re-centering device does not work. With a further increase in the relative displacement between the girder and piers, the spring and rubber will start to deform and provide a resistant force. The stiffness provided by the rubber during this process is well demonstrated with Equation (1), where G_r is shear modular, A is cross-section, and t is total rubber thickness.

$$k_r = \frac{G_r A}{t} \tag{1}$$

Now, the main work is to illustrate the lateral stiffness of the helical spring. The theoretical method is validated by the experimental and finite element methods.

2.2.1. Theoretical Method

The lateral stiffness of the helical spring is different from that in the axial direction. Specifically, axial stiffness comes from the compression or tension deformation of coils, while the lateral stiffness results from the shear deformation. The lateral stiffness of springs can be calculated by unit load method in Equation (2) [33].

$$k_{lateral} = \frac{Ed^4}{8nD^3\left[1 + \frac{4}{3}\left(\frac{L}{D}\right)^2(2+v)\right]} \tag{2}$$

$$n = \frac{Gd^4 s}{8D^3 F} \tag{3}$$

$$G = \frac{E}{2(1+v)} \tag{4}$$

where E is the modulus of elasticity; d is the nominal diameter of wire; n is the number of active coils; D is the mean diameter of coil; L is the spring length under compression; v is Poisson's ratio; G is the modulus of rigidity; s is the spring deflection; and F is the spring force.

2.2.2. Validation with Experimental and Numerical Data

To validate the helical spring's lateral stiffness, an experimental test was carried out on a TDC-C automatic compress-extension machine. The working frequency of this experimental machine ranges from 0.01 mm/min to 300 mm/min with 600 mm peak displacement, and the maximum force applied to the experimental objects was 50 kN with a working accuracy controlled within 1%. As shown in Figure 2, an internal forcing plate was set in the middle for applying force and connected to the upper kinematic device. As for the testing specimen, 55CrSiA was used to produce the experimental sample with a nominal diameter of 57.92 mm and a cross-section of 2.92 mm × 7.24 mm. Moreover, 24 coil cycles contributed to the whole length, with a relative distance between adjacent coils of 14.02 mm. The detailed information is listed in Table 1.

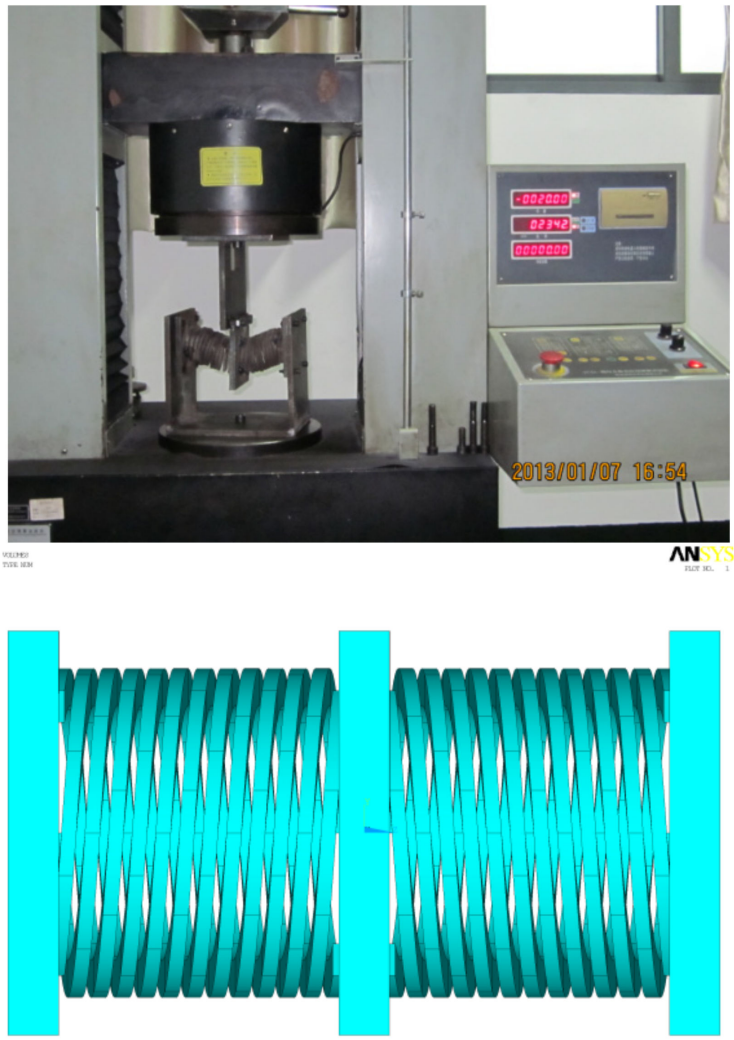

Figure 2. Experimental testing and finite element model spring.

Table 1. Detailed diameter information of the spring.

Dimension (mm)	Diameter (mm)	Distance between Adjacent Coils (mm)	Number of Coils	Material
2.92 × 7.24	57.92	14.02	24	55CrSiA

This process was also analyzed on ANSYS platform. Specifically, element type SOLID95 was used to model the characteristics of the spring. The connection between

springs and the forcing plate was modelled by Targel170 and Conta174 where the characters were determined by penalty function. The ends of the spring were fixed to steel plates at the sides. Then, the whole calculation domain was meshed into 69,120 elements with 377,850 nodes. After that, the force–displacement relationships from experimental, analytical, and theoretical approaches are plotted in Figure 3. It indicates that there are some discrepancies between them when the displacement is large. This phenomenon is attributed to the coupling effects of geometry variation and material deformation. Additionally, the practical spring provides a higher restraint stiffness than the theoretical value, which will cause a conservative re-centering effect. On the other hand, the rubber coverage provides protects to springs and avoids unstable geometry deformation. Thus, the reliability of the working states could help mitigate the discrepancies. And, the following theoretical equation can be applied to estimate the lateral spring stiffness.

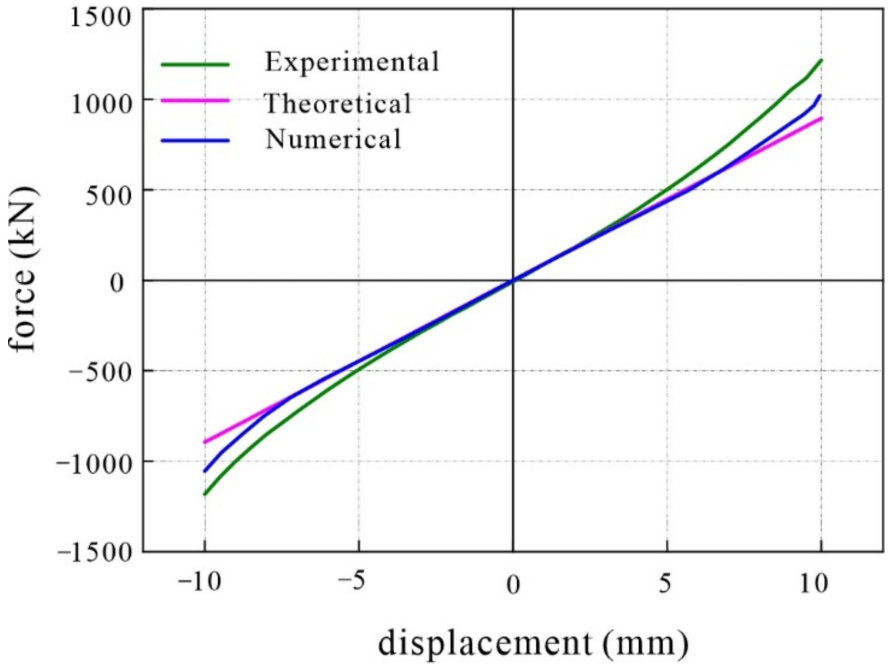

Figure 3. Force–deformation relationship of the spring in lateral direction.

3. Numerical Illustration

Finite Element Model

To evaluate the re-centering effect, a six-pylon extra-dosed cable-stayed bridge [36] was selected as an example for analysis. The symmetrical pylons of the bridge are fixed to the girder, where the girder is supported by bearings. The hybrid concrete box girder has a total length of 908 m and a width of 36.8 m. The reinforced concrete pylon was designed in a herringbone pattern in the longitudinal direction with a height of 45 m, and has nine sets of double-cable planes on each side to aid in reinforcing the girder. The average height of the reinforced concrete piers is 23 m. To avoid damages caused by extreme relative displacement between the girder and piers, 4 cable-sliding friction aseismic bearings [37] were introduced to P15 and P20, as shown in Figure 4.

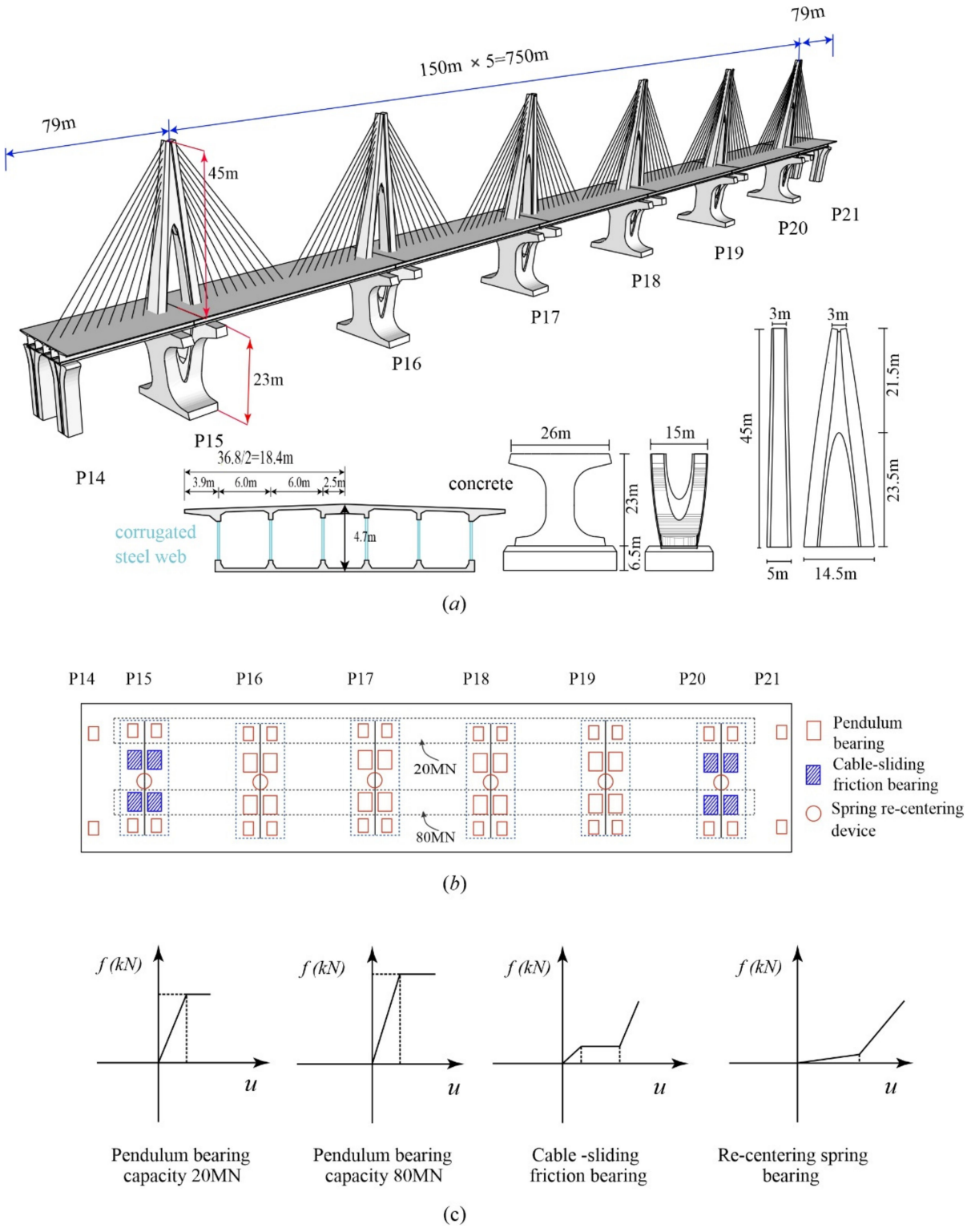

Figure 4. Schematic illustrations of bridge and the relative details (**a**) the schematic of bridge and detailed information of critical cross sections (**b**) bearing arrangement (**c**) force-displacement relationship of bearings.

The numerical model was constructed on the SAP2000 platform. Since such a huge bridge is a critical lifeline facility, the bridge was designed to remain elastic even through strong earthquakes [38–40]. Elastic frame elements were used to model the dynamic behavior of the girders, piers, and pylons. Truss elements with a modified elasticity

modulus were used to account for the sag effect of cables [41]. The local cable was assumed to be straight without further distributed mass [42]. The foundation was idealized as a six-spring model and a lumped mass is modeled at the geometric center of the pile cap [43–45]. The stiffness of the foundation spring was calculated with 'm' method and the lumped mass is the total mass of the pile cap [46–49]. To effectively demonstrate the re-centering effect of the new spring re-centering device, a multi-elastic element, which can define different stiffnesses within various working periods, was introduced to model the response of this re-centering device. Simultaneously, the force–deformation relationship of cable-sliding friction aseismic bearing was modeled by using plastic wen elements and multi-elastic elements parallelly. The free distance of cable-sliding friction aseismic bearing was 20 cm. The initial stiffness of the pendulum bearing was calculated with the classical method in Equation (5), and the restraint cable stiffness was 1.0×10^6 kN/m. The proposed re-centering device was set on all six piers. The free distance of the new spring re-centering device at each of the bridge piers was taken as 15 cm and the composed re-centering stiffness as 2.0×10^4 kN/m. It should be noted that this stiffness was a total effect of re-centering. In practical cases, this re-centering stiffness can be provided by combining several devices.

$$\begin{aligned} f_s &= \mu F_N \\ k &= \frac{f_s}{s} \end{aligned} \tag{5}$$

where μ is the friction coefficient and it usually takes 0.02, F_N is the vertical force of the bearing, s is the initial distance for the friction sliding and is 0.002 m. After that, three near-fault earthquakes (as shown in Table 2) were selected from the PEER Ground Motion Database for analysis, with magnitudes ranging from 6 to 8 and the source-to-site distance are within 10 km. These three ground motion records were applied to conduct longitudinal seismic excitation, and vertical components [50], calculated with half of the horizontal parts, were also implemented. In the present analysis, the effect of wave travelling is not of concern and only the uniform excitation is performed, where the damping ratios are determined by two critical periods (i.e., the periods of first order of modal and the one corresponding to 95% mass participant ratios) and system damping of concrete bridges.

Table 2. The selected ground motion records used for time history analysis.

No.	Seismic Wave	Recording Station	Time	Magnitude	PGA(g)
1	Cape Mendocino	Petrolia	1992	7.0	0.662
2	Chi-chi, Taiwan	TCU053	1999	7.6	0.223
3	Northridge-01	Newhall-W pico canyon rd	1994	6.7	0.325

4. Analysis Results and Discussion

The critical seismic responses in terms of shear force, moment, and displacement are recorded, where P15 (cable restraint) and P17 (general piers) present the piers with and without restraint devices. The comparison between cases with and without spring re-centering device is used to evaluate its effectiveness.

4.1. Displacement and Deformation

The maximum girder displacement in Table 3 indicates that girder displacements are similar between cases with and without the spring re-centering device. The restraints from substructures are limited when the re-centering device is installed. Figure 5 compares the relative displacement between pier P15 and decks with the excitation of earthquake waves in Table 2. We can find that the time history is almost same at the beginning, but severe discrepancies are observed at the end. The residual displacements decrease with the present spring re-centering device. This means that the restoring force works to restrict further movement when the relative displacement exceeds the initial free distance.

Table 3. Girder displacement with and without spring re-centering device.

No.	Without	With
1	0.302	0.266
2	0.276	0.259
3	0.242	0.26

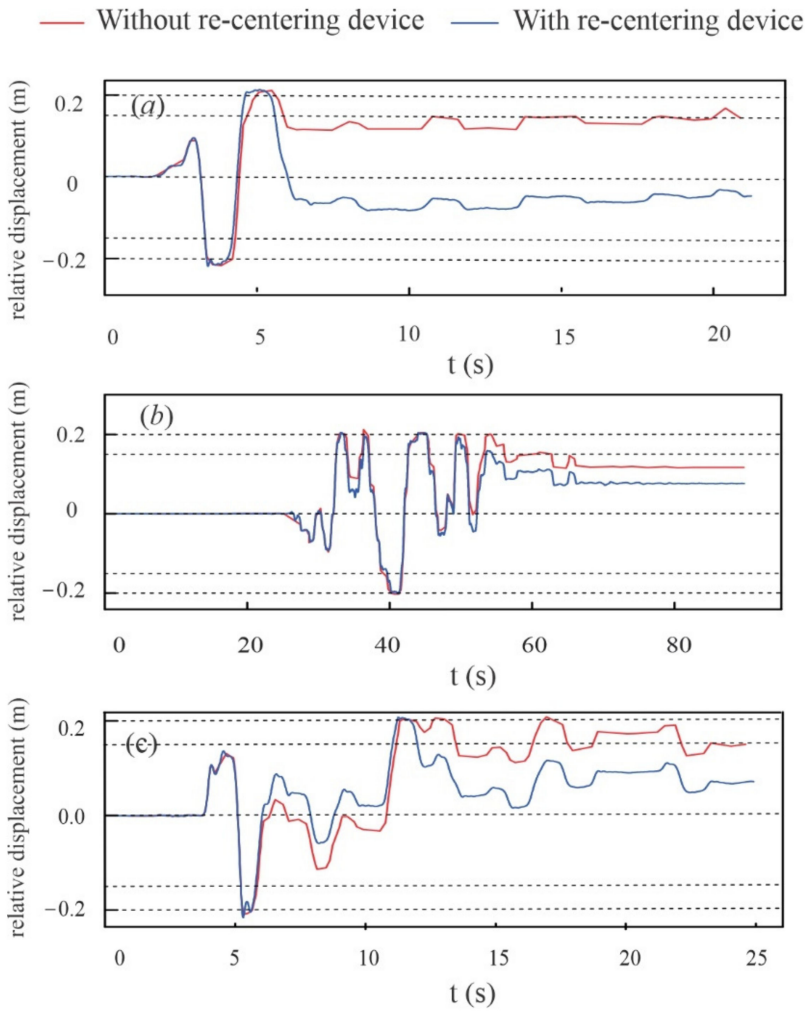

Figure 5. Relative displacement between girder and pier (**a**) Cape (**b**) Chi-Chi (**c**) Northridge.

4.2. Shear Force and Moment

Force and deformation are always concerned in engineering demand parameters during seismic analysis. Figure 6 presents the maximum shear force and moment at the bottom of the pier. We found that force on the bottom of the bridge piers decreases after a spring re-centering device is applied. The decrease of force on the piers results from the combining effect of an inertial force transformation and the variation of vibration state for substructures. As shown in Figure 5, the relative displacement between girder and pier is mitigated; this means less inertial force is transformed to the P15 and additional force is transformed to P17. On the other hand, the vibration of substructures is also impacted. For example, the hysteresis curve of cable sliding bearing is impacted by the application of such spring re-centering devices, i.e., the maximum force is decreased. Also, the installation of spring re-centering device could increase the capacity of energy dissipation. As a result, forces on pier P15 get decreased, but the mitigation effect on P17 is limited. Moreover, the bending moment at the restrained pier decreases because of mitigated shear force. However, the moment on the general pier P17 is slightly increased; this phenomenon is

explained by the fact that a larger shear force is transformed from the superstructures to the pier top.

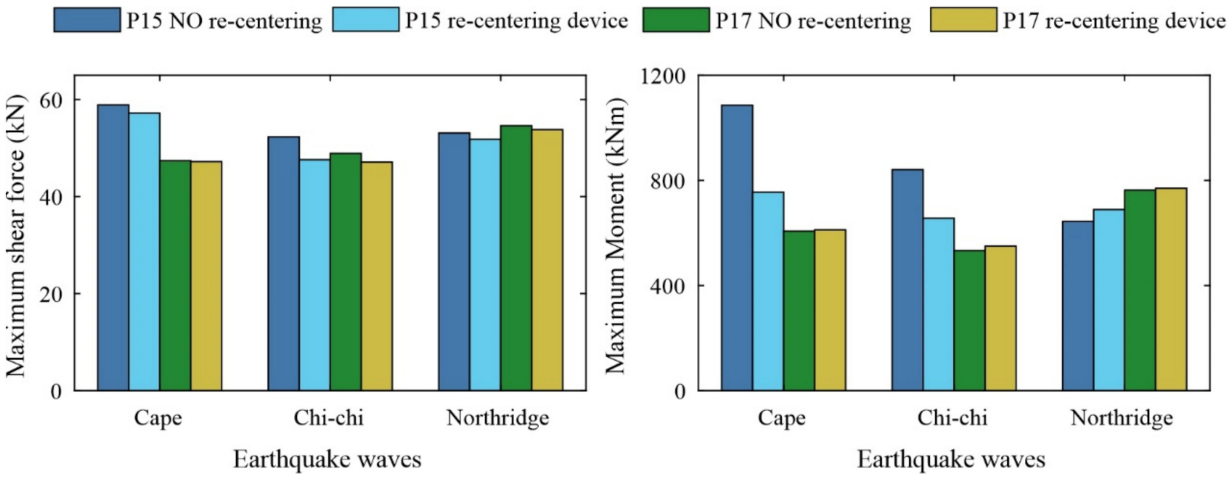

Figure 6. Shear force and bending moment at the pier bottom.

5. Parametric Analysis

To analyze the influence of the critical parameters of the spring re-centering device (initial slack and stiffness) on seismic response, an additional set of earthquakes were selected from the PEER database and a total of 10 corresponding pseudo-acceleration spectrums are depicted in Figure 7. An optimal design was carried out to investigate the impact of the critical factors. Specifically, a total 200 nonlinear time–history analysis was conducted with initial free distances 0 cm, 5 cm, 10 cm, and 15 cm, and the stiffnesses 5 MN/m, 10 MN/m, 20 MN/m, 40 MN/m and 80 MN/m.

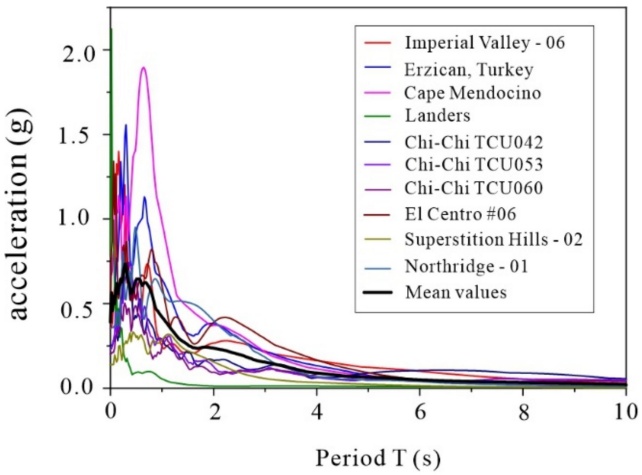

Figure 7. Pseudo-acceleration spectrum of the select ground motion.

Figure 8 indicates that the relative and residual displacement between the girder and piers increases with the rise of the initial slack values and decreases when it is constructed with a larger re-centering stiffness. We found that the bearing deformation was significant, with low restraint stiffness for all the tested initial free distances in Figure 8a. The effect of restraint stiffness has limited influence when there is a large initial slack. This means that the re-centering device does not work sufficiently and has limited impact on seismic responses. However, for the residual displacement, it increases sharply and has little impact with the restraint stiffness. It was observed that the mean residual displacement is positive around the initial slacks.

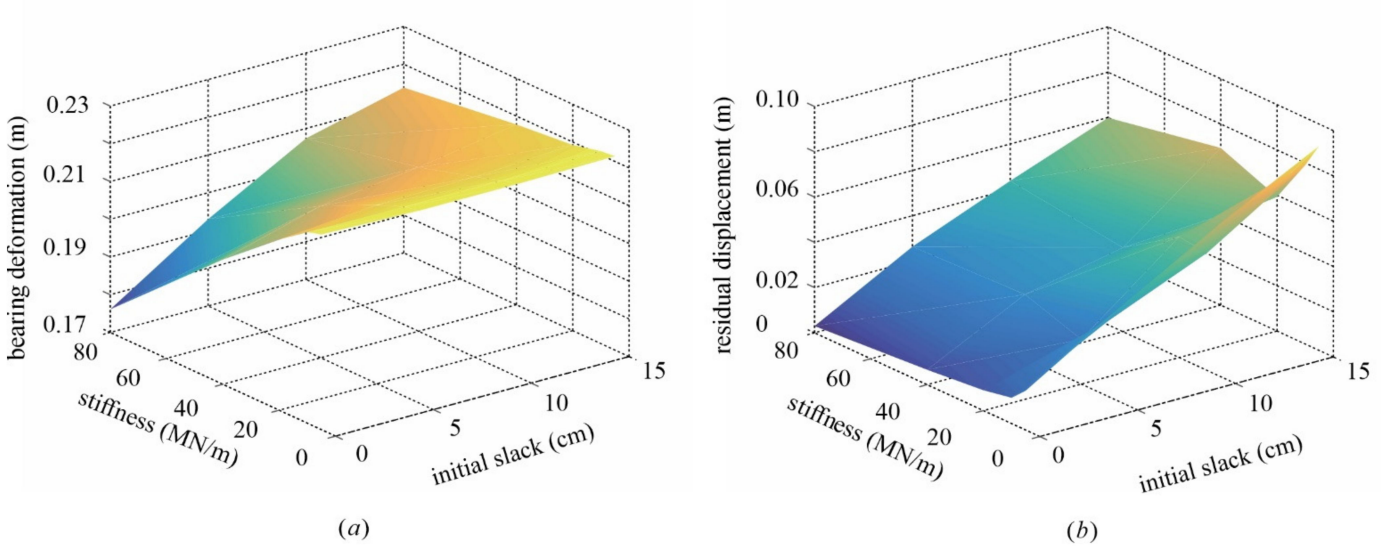

Figure 8. (**a**) Bearing deformation and (**b**) residual displacement with different design factors.

The shear force also varies with changes in initial slack and re-centering stiffness. As shown in Figure 9, there is a peak value of shear force with a 0 cm free distance and high restraint stiffness. This decreases quickly with the increase of initial free distances. For example, the shear force does not change much when the initial free distance is ranging from 10 cm to 15 cm. There is a minimum value with restraint stiffness of 40 MN/m. Additionally, the slight restraint stiffness has a limited effect on the variation of shear forces.

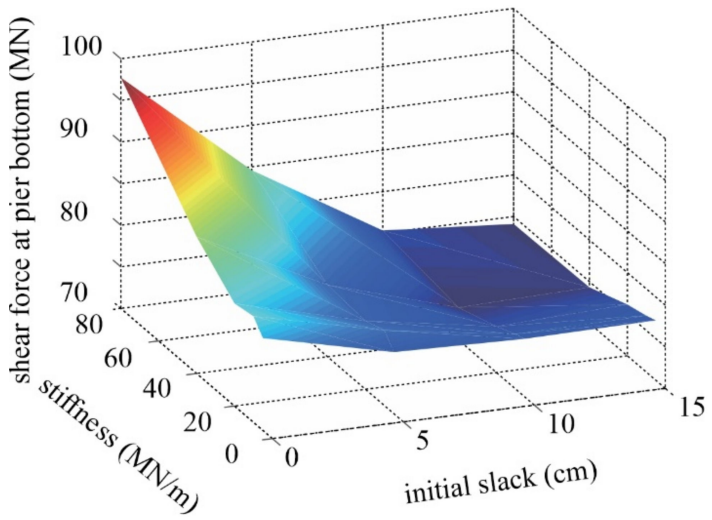

Figure 9. Peak shear force for different design factors.

6. Conclusions

The current study proposes a new spring re-centering device to increase the re-centering capacity of a sliding isolation bridge system. The working mechanism of this spring re-centering device is illustrated, while the force–deformation relationship was investigated in theoretical, experimental, and numerical methods. To assess its effect on seismic response, a three-dimensional finite element model of an extra-dosed cable-stayed bridge on SAP2000 was used to conduct analysis. Time–history analyses were carried out for bridges with and without spring re-centering devices. The shear force at the pier bottom, girder displacement, bearing deformation, and the residual displacement between girder and piers were recorded and compared.

This study indicates that sliding isolated bridge systems have an apparent residual displacement between their girder and piers after strong ground-motion excitations. The present spring re-centering device could mitigate the seismic responses and decrease residual displacement between girder and piers. The optimal design of this re-centering device demonstrates that cases with a free distance ranging from 10 cm to 15 cm correspond to the most mitigated seismic responses in terms of residual displacement and force. With such initial free distance values, the restraint stiffness has a significant influence on the residual displacement, while having relatively less impact on the shear force, bearing deformation, and girder displacement.

Author Contributions: P.Y.: conceptualization, methodology, software, validation; J.W.: formal analysis, investigation, data curation, writing—original draft preparation; Y.P.: conceptualization, writing—review and editing, visualization, funding acquisition. All authors have read and agreed to the published version of the manuscript.

Funding: This research is supported by the R & D project of China Railway Siyuan Survey and Design Institute Group Co., Ltd. (Nos. 2020k172).

Conflicts of Interest: The authors declare no conflict of interest.

References

1. Chakraborty, S.; Roy, K.; Ray-Chaudhuri, S. Design of re-centering spring for flat sliding base isolation system: Theory and a numerical study. *Eng. Struct.* **2016**, *126*, 66–77. [CrossRef]
2. Pang, Y.; He, W.; Zhong, J. Risk-based design and optimization of shape memory alloy restrained sliding bearings for highway bridges under near-fault ground motions. *Eng. Struct.* **2021**, *241*, 112421. [CrossRef]
3. Cao, S.; Ozbulut, O.E.; Shi, F.; Deng, J. Experimental and numerical investigations on hysteretic response of a multi-level SMA/lead rubber bearing seismic isolation system. *Smart Mater. Struct.* **2022**, *31*, 035024. [CrossRef]
4. Deng, J.; Hu, F.; Ozbulut, O.E.; Wu, S.; Sun, Z.; Cao, S. Verification of multi-level SMA/lead rubber bearing isolation system for seismic protection of bridges. *Soil Dyn. Earthq. Eng.* **2022**, *161*, 107380. [CrossRef]
5. Chen, X.; Xiong, J. Seismic resilient design with base isolation device using friction pendulum bearing and viscous damper. *Soil Dyn. Earthq. Eng.* **2022**, *153*, 107073. [CrossRef]
6. Xiang, N.; Alam, M.S. Comparative seismic fragility assessment of an existing isolated continuous bridge retrofitted with different energy dissipation devices. *J. Bridge Eng.* **2019**, *24*, 04019070. [CrossRef]
7. Xiang, N.; Alam, M.S. Displacement-based seismic design of bridge bents retrofitted with various bracing devices and their seismic fragility assessment under near-fault and far-field ground motions. *Soil Dyn. Earthq. Eng.* **2019**, *119*, 75–90. [CrossRef]
8. Li, S.; Dezfuli, F.H.; Wang, J.; Alam, M.S. Seismic vulnerability and loss assessment of an isolated simply-supported highway bridge retrofitted with optimized superelastic shape memory alloy cable restrainers. *Bull. Earthq. Eng.* **2020**, *18*, 3285–3316. [CrossRef]
9. Cao, S.; Ozbulut, O.E.; Shi, F.; Deng, J. An SMA cable-based negative stiffness seismic isolator: Development, experimental characterization, and numerical modeling. *J. Intell. Mater. Syst. Struct.* **2022**, *33*, 1819–1833. [CrossRef]
10. Chen, X.; Ikago, K.; Guan, Z.; Li, J.; Wang, X. Lead-Rubber-Bearing with Negative Stiffness Springs (LRB-NS) for Base-Isolation Seismic Design of Resilient Bridges: A Theoretical Feasibility Study. *Eng. Struct.* **2022**, *266*, 114601. [CrossRef]
11. Zhou, L.; Wang, X.; Ye, A. Shake table test on transverse steel damper seismic system for long span cable-stayed bridges. *Eng. Struct.* **2019**, *179*, 106–119. [CrossRef]
12. Li, S.; Wang, J.; Alam, M.S. Seismic performance assessment of a multispan continuous isolated highway bridge with superelastic shape memory alloy reinforced piers and restraining devices. *Earthq. Eng. Struct. Dyn.* **2021**, *50*, 673–691. [CrossRef]
13. Yi, J.; Zhou, J.; Ye, X. Seismic control of cable-stayed bridge using negative stiffness device and fluid viscous damper under near-field ground motions. *J. Earthq. Eng.* **2022**, *26*, 2642–2659. [CrossRef]
14. Wei, B.; Hu, Z.; He, X.; Jiang, L. System-based probabilistic evaluation of longitudinal seismic control for a cable-stayed bridge with three super-tall towers. *Eng. Struct.* **2021**, *229*, 111586. [CrossRef]
15. Li, C.; Yang, L.; Li, H. Fragility assessment and optimum design of a steel–concrete frame structure with hybrid energy-dissipated devices under multi-hazards of earthquake and wind. *Eng. Struct.* **2021**, *245*, 112878. [CrossRef]
16. Pang, Y.; Sun, Y.; Zhong, J. Resilience-based performance and design of SMA/sliding bearing isolation system for highway bridges. *Bull. Earthq. Eng.* **2021**, *19*, 6187–6211. [CrossRef]
17. Pang, Y.; Wang, X. Cloud-IDA-MSA conversion of fragility curves for efficient and high-fidelity resilience assessment. *J. Struct. Eng.* **2021**, *147*, 04021049. [CrossRef]
18. Pranesh, M.; Sinha, R. VFPI: An isolation device for aseismic design. *Earthq. Eng. Struct. Dyn.* **2000**, *29*, 603–627. [CrossRef]
19. Hamidi, M.; El Naggar, M.H.; Vafai, A.; Ahmadi, G. Seismic isolation of buildings with sliding concave foundation (SCF). *Earthq. Eng. Struct. Dyn.* **2003**, *32*, 15–29. [CrossRef]

20. Fenz, D.M.; Constantinou, M.C. Spherical sliding isolation bearings with adaptive behavior: Theory. *Earthq. Eng. Struct. Dyn.* **2008**, *37*, 163–183. [CrossRef]
21. Mostaghel, N.; Khodaverdian, M. Dynamics of resilient-friction base isolator (R-FBI). *Earthq. Eng. Struct. Dyn.* **1987**, *15*, 379–390. [CrossRef]
22. Zayas, V.A.; Low, S.A.; Mahin, S.A. *The FPS Earthquake Resisting System Experimental Report*; Earthquake Engineering Research Center: Oakland, CA, USA, 1987.
23. Haque, A.B.M.R.; Alam, M.S. Hysteretic Behaviour of a Piston Based Self-centering (PBSC) Bracing System Made of Superelastic SMA Bars–A Feasibility Study. *Structures* **2017**, *12*, 102–114. [CrossRef]
24. Cao, S.; Ozbulut, O.E.; Wu, S.; Sun, Z.; Deng, J. Multi-level SMA/lead rubber bearing isolation system for seismic protection of bridges. *Smart Mater. Struct.* **2020**, *29*, 055045. [CrossRef]
25. Cao, S.; Ozbulut, O.E. Long-stroke shape memory alloy restrainers for seismic protection of bridges. *Smart Mater. Struct.* **2020**, *29*, 115005. [CrossRef]
26. Ozbulut, O.E.; Hurlebaus, S. Re-centering variable friction device for vibration control of structures subjected to near-field earthquakes. *Mech. Syst. Signal Process.* **2011**, *25*, 2849–2862. [CrossRef]
27. Kitayama, S.; Constantinou, M.C. Probabilistic collapse resistance and residual drift assessment of buildings with fluidic self-centering systems. *Earthq. Eng. Struct. Dyn.* **2016**, *45*, 1935–1953. [CrossRef]
28. Kitayama, S.; Constantinou, M.C. Seismic response analysis of single-degree-of-freedom yielding structures with fluidic self-centering systems. *Eng. Struct.* **2016**, *125*, 266–279. [CrossRef]
29. Constantinou, M.C.; Mokha, A.S.; Reinhorn, A.M. Study of sliding bearing and helical-steel-spring isolation system. *J. Struct. Eng.* **1991**, *117*, 1257–1275. [CrossRef]
30. Constantinou, M.; Mokha, A.; Reinhorn, A. Teflon bearings in base isolation II: Modeling. *J. Struct. Eng.* **1990**, *116*, 455–474. [CrossRef]
31. Xu, L.; Fan, X.; Li, Z. Experimental behavior and analysis of self-centering steel brace with pre-pressed disc springs. *J. Constr. Steel Res.* **2017**, *139*, 363–373. [CrossRef]
32. Khoo, H.H.; Clifton, C.; Butterworth, J.; MacRae, G. Experimental study of full-scale self-centering sliding hinge joint connections with friction ring springs. *J. Earthq. Eng.* **2013**, *17*, 972–997. [CrossRef]
33. Wang, S.J.; Yang, Y.H.; Lin, F.R.; Jeng, J.W.; Hwang, J.S. Experimental Study on Seismic Performance of Mechanical/Electrical Equipment with Vibration Isolation Systems. *J. Earthq. Eng.* **2017**, *21*, 439–460. [CrossRef]
34. Guo, W.; Li, J.; Guan, Z.; Chen, X. Pounding performance between a seismic-isolated long-span girder bridge and its approaches. *Eng. Struct.* **2022**, *262*, 114397. [CrossRef]
35. Zhong, J.; Yang, T.; Pang, Y.; Yuan, W. A novel structure-pulse coupled model for quantifying the column ductility demand under pulse-like GMs. *J. Earthq. Eng.* **2021**, 1–19. [CrossRef]
36. Yang, H.; Pang, Y.; Tian, S.; Dang, X.; Yuan, W. Case study of the seismic response of an extra-dosed cable-stayed bridge with cable-sliding friction aseismic bearing using shake table tests. *Struct. Des. Tall Spec. Build.* **2017**, *26*, e1398. [CrossRef]
37. Yuan, W.; Wang, B.; Cheung, P.; Cao, X.; Rong, Z. Seismic performance of cable-sliding friction bearing system for isolated bridges. *Earthq. Eng. Eng. Vib.* **2012**, *11*, 173–183. [CrossRef]
38. Pang, Y.; Wu, X.; Shen, G.; Yuan, W. Seismic fragility analysis of cable-stayed bridges considering different sources of uncertainties. *J. Bridge Eng.* **2014**, *19*, 04013015. [CrossRef]
39. Li, C.; Li, H.N.; Hao, H.; Bi, K.; Chen, B. Seismic fragility analyses of sea-crossing cable-stayed bridges subjected to multi-support ground motions on offshore sites. *Eng. Struct.* **2018**, *165*, 441–456. [CrossRef]
40. Wei, K.; He, H.; Zhang, J.; Yang, C.; Qin, S. An endurance time method-based fragility analysis framework for cable-stayed bridge systems under scour and earthquake. *Ocean Eng.* **2021**, *232*, 109128. [CrossRef]
41. Pang, Y.; Wei, K.; He, H.; Wang, W. Assessment of lifetime seismic resilience of a long-span cable-stayed bridge exposed to structural corrosion. *Soil Dyn. Earthq. Eng.* **2022**, *157*, 107275. [CrossRef]
42. Zhang, Y.Y.; Ding, Y.; Pang, Y.T. Selection of optimal intensity measures in seismic damage analysis of cable-stayed bridges subjected to far-fault ground motions. *J. Earthq. Tsunami* **2015**, *9*, 1550003. [CrossRef]
43. Li, S.; Zhang, F.; Wang, J.; Alam, M.S.; Zhang, J. Seismic responses of super-span cable-stayed bridges induced by ground motions in different sites relative to fault rupture considering soil-structure interaction. *Soil Dyn. Earthq. Eng.* **2017**, *101*, 295–310. [CrossRef]
44. Zhong, J.; Ni, M.; Hu, H.; Yuan, W.; Yuan, H.; Pang, Y. Uncoupled multivariate power models for estimating performance-based seismic damage states of column curvature ductility. *Structures* **2022**, *36*, 752–764. [CrossRef]
45. Chen, X.; Xiang, N.; Guan, Z.; Li, J. Seismic vulnerability assessment of tall pier bridges under mainshock-aftershock-like earthquake sequences using vector-valued intensity measure. *Eng. Struct.* **2022**, *253*, 113732. [CrossRef]
46. Zhuang, L.; Yin, P.; Pang, Y. E-Cloud: Efficient seismic fragility assessment of structures based on enhanced cloud analysis. *Earthq. Spectra* **2022**, 1–19. [CrossRef]
47. Pang, Y.; Meng, R.; Li, C.; Li, C. A probabilistic approach for performance-based assessment of highway bridges under post-earthquake induced landslides. *Soil Dyn. Earthq. Eng.* **2022**, *155*, 107207. [CrossRef]
48. Fan, W.; Zhong, Z.; Huang, X.; Sun, W.; Mao, W. Multi-platform simulation of reinforced concrete structures under impact loading. *Eng. Struct.* **2022**, *66*, 114523. [CrossRef]

49. Zhang, N.; Zhang, Y.; Gao, Y.; Pak, R.Y.; Yang, J. Site amplification effects of a radially multi-layered semi-cylindrical canyon on seismic response of an earth and rockfill dam. *Soil Dyn. Earthq. Eng.* **2019**, *116*, 145–163. [CrossRef]
50. Dai, D.; El Naggar, M.H.; Zhang, N.; Wang, Z. Rigorous solution for kinematic response of floating piles subjected to vertical P-wave. *Appl. Math. Model.* **2022**, *106*, 114–125. [CrossRef]